Eur. Phys. J. Plus (2025) 140:547
https://doi.org/10.1140/epjp/s13360-025-06356-3

THE EUROPEAN PHYSICAL JOURNAL PLUS

Regular Article

The study of two impressive *simulacra* at Santa Casa da Misericórdia de Almada, Portugal

Teresa Ferreira[1,2,a], **Margarida Nunes**[1,b], **Ana Curto**[1], **Joana Palmeirão**[1,3], **Ana Manhita**[1], **Fernanda Olival**[4,5], **Luís Piorro**[6], **Paula Monteiro**[6], **Eduarda Vieira**[3]

[1] HERCULES Laboratory/IN2PAST, University of Évora, Largo Marquês de Marialva 8, Évora, Portugal
[2] Chemistry and Biochemistry Department, Sciences and Technology School, University of Évora, Rua Romão Ramalho 59, Évora, Portugal
[3] Research Center for the Science and Technology of the Arts (CITAR), School of Arts, Universidade Católica Portuguesa, Rua de Diogo Botelho 1327, Porto, Portugal
[4] CIDEHUS, Palácio do Vimioso, University of Évora, Largo Marquês de Marialva 8, Évora, Portugal
[5] History Department, Social Sciences School, University of Évora, Largo dos Colegiais 2, Évora, Portugal
[6] Laboratório José de Figueiredo, Museus e Monumentos de Portugal, Rua das Janelas Verdes, Lisbon, Portugal

Received: 15 November 2024 / Accepted: 23 April 2025

Abstract Simulacra, or full-body reliquaries of *corpi santi*, have largely been overlooked in the discourse of the past century by the Church, the general public, and scholars. This work investigates two noteworthy cases among simulacra—two young individuals, St. Primogenita and St. Theodore—from Santa Casa da Misericórdia de Almada in Portugal. Based on a historical and analytical approach, the study examines the *simulacra* context, assembly methods, materials, symbols of martyrdom, and adornments. Their possible arrival in Portugal in the late eighteenth century is supported by the Bishop's seal and textile features that reflect the fashion of that period. Radiographic imaging and particularly borescope inspections revealed distinct assembly techniques, with St. Theodore displaying meticulous anatomical assembly, while St. Primogenita's construction is less precise. However, access to the cranium fragments of St. Primogenita revealed an elaborate consolidation method. SEM–EDS, FT-IR, and Py-GC–MS analyses identified a fibrous material coated with a dark brown paste, likely used to bond the unfused parts of the ectocranium fragments of a young individual, as well as a paste applied to reinforce the endocranium. Martyrdom symbols further distinguished the *simulacra*, with St. Primogenita adorned with a silk petal crown attached using animal glue, whereas St. Theodore's crown was crafted from pigment-dyed cellulosic materials. LC-DAD-MS analysis revealed the natural dyes used in coloured threads. Only St. Primogenita retained fragments from a phial of blood, where a creative method may have been employed to emphasise the blood content. This investigation highlighted the complexity and artistry behind these *simulacra*.

1 Introduction

In the early centuries of Christianity, Christians often refused to comply with imperial mandates, like performing animal sacrifices or participating in the imperial cult. Instead, they remain steadfast in their beliefs, even in persecution and martyrdom [1–3]. As the early Church emerged, the cult of relics developed, reflecting care for the remains of those who died for their faith while establishing a spiritual connection with their souls [4].

Rooted in Jewish burial practices, the respect for the human body and driven by urban overpopulation and land shortages, underground burial grounds known as catacombs emerged in Rome from the second to the fifth centuries AD. Interestingly, most burials occurred in the fourth and fifth centuries, after the Edict of Milan in 313 AD, when policies towards Christians changed [5]. However, these sites were largely forgotten until their rediscovery in the late sixteenth century.

The same century brought upheavals of the Protestant Reformation, a period of intense criticism of Catholic practices, including the veneration of relics. The Catholic response, shaped by the Council of Trent, reformed the cult of saints, making relics central to Baroque piety, especially in Roman-aligned regions [6]. In 1578, a major turning point occurred when an undisturbed burial site was discovered near the Salaria Gate in Rome. Many mistakenly believed the catacombs mainly housed martyrs, resulting in rampant openings of *loculi* and the transfer of remains, called holy bodies (*corpi santi*) or catacomb saints. This unregulated activity prompted papal edicts to restrict unauthorised access and excavations by the end of the sixteenth century [7].

[a] e-mail: tasf@uevora.pt (corresponding author)
[b] e-mail: mrmpn@uevora.pt (corresponding author)

Published online: 18 June 2025

To bring order to this growing practice, Pope Clement IX established the Congregation for Indulgences and Sacred Relics in the late seventeenth century, which had previously defined two key proofs of martyrdom: the depiction of the palm leaf on the *loculus* inscription and a phial believed to contain the martyr's blood (*vas sanguinis*). The Cardinal Vicar of Rome was granted authority over the catacombs, with the power to order excavations and define procedures for extracting, preserving, and distributing martyrs' relics. These relics were stored in a Lipsanotheca, overseen by a Custodian of the Sacred Relics, who distributed them to the clergy and faithful, except for those selected for the Monsignor Sacristan, Titular Bishop of Porphyreon, the first and principal officer of the papal chapel [8].

The cult of the holy bodies experienced a significant surge between the seventeenth and nineteenth centuries, resulting in widespread exhumations and scepticism about the relics' authenticity [7].

Initially, the bone remains, sometimes entire bodies, were transported in simple wooden boxes or ornate containers without anatomical reconstructions and accompanied by *authentica* documents. Some relics were placed in more elaborate reliquaries, where bones were sometimes arranged in intricate formations, adorned with colourful flowers or papier-mâché garlands. From the eighteenth century onward, the reconstruction of skeletons in anatomical configurations and dressed in elaborate garments adorned with beads and stones became widespread. These striking visual displays significantly impacted the faithful and contributed to the spread of *simulacra* throughout Catholic Europe and the Americas [9]. *Simulacra* elevated local churches into devotion centres, enhancing parish prestige while fuelling rivalries among parishes [10, 11].

Relics are often perceived as undervaluable or macabre objects, garnering little attention in the study of natural and physical sciences. Their sacred status also demands research methods that align with Catholic Church protocols, making analysis more complex. Scientific examinations are often only possible during restoration projects [12]. Occasionally, the Church itself restricts such analysis. However, in recent years, Church authorities have shown a growing openness to scientific investigation of relics [13–15].

Most research on relics and their reliquaries has remained within historical or art-historical contexts [12, 16, 17]. Only a limited number of studies, mainly conducted in Europe, have addressed their analytical examination or conservation. These studies, such as academic theses and scientific publications, highlight the importance of integrating methodologies from the physical sciences to understand the material composition and construction techniques of holy bodies as *simulacra* [13, 18–20]. Among these, non-invasive methods such as computed tomography and conventional or digital radiography have been employed for anthropological evaluation, as direct access to skeletal remains is often restricted. A notable example is the study by Kristóf and co-authors [21], the first radiological examination in central Europe. With an emphasis on paleoradiology, the authors used conventional radiography and computed tomography to assess the skeletal remains of the martyrs' saints Christina and Augustine in Hungary. The radiological examinations provided insights into the internal features of the skeletons, including their assembly techniques and conservation state, as well as details of their external garments, such as embroidery, lace, and metallic decorations. These findings contributed to the conservation and restoration plan later developed by specialists. More recently, Sánchez Reyes [10, 22] conducted the first systematic radiographic study on *simulacra* from Mexico, primarily to understand their assemblage. By integrating archival insights, the author attested that local productions existed alongside the large-scale donations from Rome to Mexico. Endoscopic examinations have also provided further insights into the internal assembly and potential modifications carried out over time. Particularly noteworthy is Pfeiffer's doctoral dissertation [23], which emphasises the technical and material aspects of nine *simulacra* preserved in museums and monasteries across Germany. Known to be assembled in female monastic workshops, these *simulacra* contain adhesives, textiles, paper, parchment, and wax, among others. The study shed light on both the original construction techniques and subsequent restoration interventions. Radiocarbon dating was a crucial method for establishing the chronological context of the relics. The analyses indicated that relics date back to the early centuries of Christianity rather than being sourced from local mediaeval or early modern burial sites for forgery [24]. However, no further analyses were performed [14, 15, 21, 24]. A recent study focussed on the relics of the apostles St. James and St. Philip, housed in the Basilica dei Santi Apostoli in Rome [25]. Although these relics are neither *simulacra* nor likely to have originated from the Roman catacombs, the investigation stands as a notable example of a comprehensive, multi-analytical approach to the study of early martyr relics. Researchers examined both bone and mummified remains, as well as architectural components, using a range of scientific techniques, including radiocarbon and thermoluminescence dating, chromatography, mass spectrometry, and X-ray diffraction and infrared spectroscopy. The findings revealed that the relics had undergone multiple conservation and exhibition treatments, and notably, the femoral bone attributed to St. James was dated to a period that excludes its authenticity as belonging to the apostle. In the national context, Palmeirão's PhD [19] was a pioneering study that mapped 56 *simulacra* across the country and characterised more than a dozen. This work offered valuable insights into the *simulacra* historical periods and places of origin, as well as their conservation state, along with proposed conservation protocols.

This work employed a holistic approach to investigate two catacomb saints in Portugal, purportedly martyrs from the Roman Empire buried in the Roman catacombs. Notably, these martyrs are children, a rare occurrence among *simulacra*. The objective was to deconstruct the various materials used in their creation and value the intricate craftsmanship involved. Non-invasive in situ techniques, such as digital radiography and borescope inspection, were employed to assess the completeness, conservation state, anatomical correctness, and individuality of the bones, as well as the internal structure shaping the bodies and reliquary adornments, suggesting stylistic differences and specialised expertise. When possible, samples were collected for in-lab techniques, including radiocarbon dating, gas and liquid chromatographies, optical and scanning electron microscopies, and infrared spectroscopy. Optical and scanning electron microscopy combined with chemical analysis (SEM–EDS) facilitated a detailed examination of the various

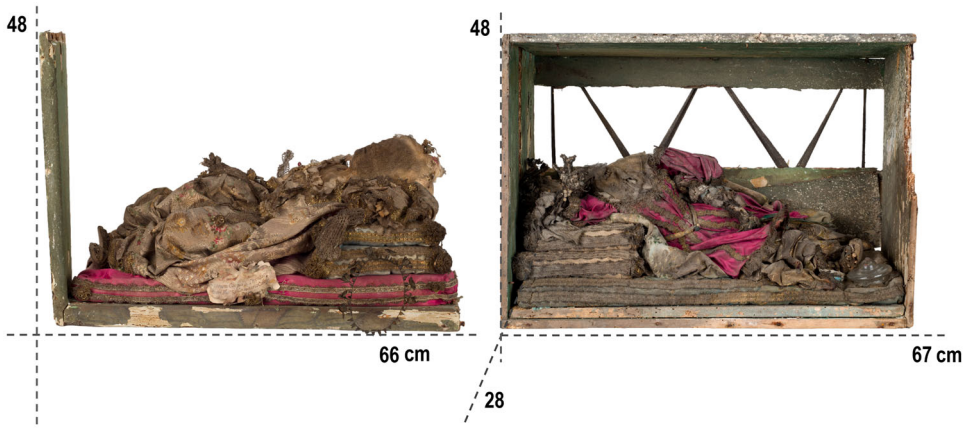

Fig. 1 *Simulacra* of St. Theodore (left) and St. Primogenita (right) with the dimensions of the urns

samples, shedding light on original craftsmanship and degradation processes of metal threads, among others. Chromatographic techniques, such as high-performance liquid chromatography with diode array and mass spectrometry detection (HPLC–DAD-MS) and pyrolysis–gas chromatography coupled with mass spectrometry (Py-GC–MS), were employed to identify organic materials, including natural dyes used in the garments and other textile objects, as well as binding materials for the face and skull assemblage. Infrared spectroscopy played a crucial role as a preliminary or complementary approach to Py-GC–MS for analysing pastes, resins, adhesives, and other organic substances.

Overall, the analyses aimed to date the bone and characterise the contents of the urns, which included flower crowns, a phial of blood, beads, a paper cartouche, and textiles from garments, mattresses, and cushions. Material analysis revealed the use of high-quality textiles, intricate metal frameworks and sophisticated techniques, emphasising the artistic and devotional significance of these objects.

By employing advanced diagnostic approaches, this study provided a comprehensive understanding of both the tangible and intangible aspects of catacomb saints, bridging the gap between historical narratives and material evidence. The research sought to uncover a forgotten heritage, laying the groundwork for the conservation and musealisation of these items, even within sacred spaces, ensuring their cultural value is preserved.

2 Material and methods

2.1 Sampling

Two *corpi santi*, represented as *simulacra* (Fig. 1), were analysed. Sampling was conducted in areas that did not compromise the integrity of the items, such as loose or partially detached threads from the textiles. In total, 30 samples from St. Theodore and 27 samples from St. Primogenita were collected and categorised into three material types (Table 1):

a. materials in direct contact with bones: gauze, cotton, paper, and pastes;
b. textiles: metal threads and dyed fibres in various colours used for the garments, such as mantles, dresses, and skirt, as well as mattresses and cushions;
c. symbols of martyrdom and decorative elements: a phial of blood, flower crowns, beads, and a paper cartouche bearing the name of the *simulacrum* (St. Theodore).

2.2 Instrumentation and analysis

2.2.1 Visual inspection of simulacra and samples

Digital photography

The photographic documentation was done with a Mamiya RZ67 Pro II camera equipped with a Mamiya-Sekor 65 mm f:4 lens, a Sinar 44 sensor, and tungsten illumination (2×1000 W).

Digital microscopy

High-resolution digital microscopy was conducted with a 3D Hirox RH-2000 digital microscope (©Hirox Europe, France) equipped with an MXB-5040RZRZ revolver zoom lens. Images were acquired from $140\times$ to $400\times$ magnifications, with top-light illumination and Hirox™ software.

Dark-field (DFM) and bright-field (BFM) microscopies

Table 1 Sample identification code (ID), item (e.g. garment, decorative element, symbol of martyrdom), and a brief description of the samples collected from St. Theodore and St. Primogenita

	Sample ID	Item	Type	Description	Colour
St. Theodore	T1	Dress	Paste	Small beads	Beige
	T2	Flower crown	Fabric	Petals	Green and yellow
	T3	Paper cartouche	Cartouche	Paper with ink	Off-white
	T4*	Face	Textile fibre with a solid residue attached	Gauze, silk fibre | weft and warp with a solid residue integrated into the material	Greyish tone
	T5	Dress	Paste	Beads	Beige
	T6	Mantle	Metal thread	Strip	Gilt strip
	T8	Mantle	Metal thread	Strip wound around a silk core	Gilt strip yellow core
	T10	Mantle	Textile fibre	Warp	Pink
	T11	Mantle	Textile fibre	Weft	Pink
	T12	Mantle	textile fibre	Floral motifs | weft	Light green
	T13	Mantle	Textile fibre	Floral motifs | weft	Green
	T14	Mantle	Textile fibre	Floral motifs | weft	Orange
	T15	Mantle	Textile fibre	Floral motifs | weft	Brown
	T16	Mantle	Textile fibre	Floral motifs | weft	Blue
	T17	Mantle	textile fibre	Floral motifs | weft	Dark orange
	T18	Mantle	Metal thread	Strip wound with a silk thread	Silver strip red core
	T18a	mantle	Textile fibre	Crimp weft thread	White
	T19	Dress	Metal thread	Weft strip	Silver strip
	T20	Dress	Metal thread	Strip wound around a silk thread	Silver strip white core
	T21	Dress	Textile fibre	Floral motifs | weft	Green
	T22	Dress	Textile fibre	Floral motifs | weft	Yellow
	T23	Dress	Textile fibre	Floral motifs | weft	Brown
	T23a	Dress	Textile fibre	Floral motifs | weft	Red
	T23b	Dress	Metal thread	STRIP wound with a crimped silk thread	Silver strip yellow core
	T26	Dress sleeve	Metal thread	Lace | strip wound around a silk core	Gilt strip yellow core
	T27	Face	Textile thread	Gauze, warp	Greyish tone
	T28	Face	Textile thread	Gauze, weft	Greyish tone
	T29	Glove	Metal thread	Strip wound around a silk core	Silver strip white core
	T30	Ectocranium	Residues	Occipital bone	White
	T31	Head/cranium	Textile thread	Cotton filling	White
St. Primogenita	P1	Flower crown	Fabric	Petal	Red
	P4	Dress	Paste	Beads	Beige
	P5	Dress	Textile thread	Warp	Yellow
	P6	Dress	Textile thread	Weft	Pink
	P7a	Mattress	Textile thread	Warp	Blue
	P7v	Mattress	Textile thread	Warp	Light blue
	P8	Mattress	Textile thread	Floral motifs | weft	Yellow
	P10	Mattress	Textile thread	Floral motifs | weft	Green
	P11	Mantle	Textile thread	Weft (wrong side)	Light blue
	P13	Mantle	Textile thread	Floral motifs | weft	Green
	P15	Mantle	Textile thread	Floral motifs | weft	Light green
	P16	Mantle	Textile thread	Weft (right side)	Multicoloured blue
	P18	Mantle	Metal thread	Weft strip	Silver strip
	P19	Mantle	Metal thread	Floral motifs | strip wound around a silk core	Gilt strip green silk

Table 1 continued

Sample ID	Item	Type	Description	Colour
P21	Skirt	Textile thread	Floral motifs | weft	Green
P22	Skirt	Textile thread	Floral motifs | weft	Light blue
P23	Skirt	Textile thread	Floral motifs | weft	Blue
P25	Skirt	Textile thread	Floral motifs | weft	Pink
P29	Skirt	Metal thread	Strip wound around a silk core	Gilt strip yellow core
P31	Skirt	Metal thread	Strip	Gilt strip
P33	Chest	Textile thread	Gauze, warp	Greyish tone
P34	Chest	Textile thread	Gauze, weft	Greyish tone
P35	Dress hem	Metal thread	Lace | strip wound around a medium silk core	Gilt strip yellow core
P36	Dress hem	Metal thread	Lace | strip	Gilt strip
P38*	Ectocranium	Paste over cellulose fibres	Fragment	Dark brown
P39*	endocranium	Cement-like material	Fragment	Light brown
P40	Phial of blood	Glass object	Ambar layer and brown residue	Ambar, dark brown

T4*: the solid residue attached to the silk fibres was separated using micro tweezers under a stereomicroscope, and the residue was collected for further analysis
P38*: a similar procedure was employed to separate the dark brown paste from the cellulose fibres for additional analysis
P39*: a similar procedure was used to remove the cement-like material from the endocranium sample for further analysis

A Leica DM2500M dark-field microscope (©Leica Microsystems GmbH, German) paired with a Leica MC170 HD digital camera and a Meiji MT bright-field (©Meiji Techno, Japan) microscope coupled to a Dino-Eye eyepiece camera (©AnMo Electronics Corporation, Taiwan) were utilised for the observation and imaging of textile fibres at magnifications of 100× and 200× . For longitudinal observation, the textile fibres were carefully separated and placed on a glass slide with a drop of water.

2.2.2 Evaluation of the internal structure and bones

In situ radiographic imaging

In situ digital radiographic imaging was conducted using a Yxlon Andrex Smart 160e portable X-ray generator tube and a Scanna CR35 digitisation system. The X-ray source was positioned at a distance of 310 cm from the X-ray plates, which were placed behind the *simulacra*, completely covering the artefact. In addition to full-body image acquisition, partial head, pelvis, and feet exposures were performed. The images were obtained at 30 kV and 40 kV voltage, with a current of 5 mA, with 5 and 10 min acquisition, respectively.

Borescope inspection

The interior of the *simulacra* was inspected using a portable borescope (ChiliTec GmbH, Lehre). The device was carefully introduced through apertures in the chest, arms, and legs whenever accessible. The movement was executed slowly and steadily, allowing the camera to capture detailed images without blurring. The borescope was connected to a laptop for real-time viewing, enabling the capture of high-resolution images and videos for subsequent analysis. This borescope features a 1080P resolution, a semi-rigid 5-m USB cable, an 8 mm diameter lens, and six adjustable LED lights to enhance visibility during the inspection.

2.2.3 Analytical characterisation of the samples

Radiocarbon dating

A cranium fragment from the partially damaged *simulacrum* of St. Primogenita was analysed for radiocarbon dating at the Vilnius Radiocarbon Laboratory. The sample underwent an acid–base-acid pre-treatment and collagen extraction protocol to remove contaminants and isolate the organic fraction. Graphitisation was performed using Automated Graphitisation Equipment AGE-3 (Ionplus AG, Zürich). Radiocarbon measurements were then conducted using a single stage accelerator mass spectrometer (SSAMS, NEC). Calibration employed reference materials NIST-OXII and phthalic anhydride to ensure accurate dating estimation. It was not possible to collect a bone sample from St. Theodore to perform radiocarbon dating due to the necessity of partial destruction of the *simulacrum* to access the bones.

Fourier transform infrared spectroscopy with attenuated total reflection (FT-IR-ATR)

The ATR-FT-IR analyses were conducted using a Bruker Alpha spectrometer (Bruker™ Optics and Microanalysis GmbH, Germany), operated with OPUS 6.5 software. Spectra were collected in the region 4000–350 cm^{-1} region with a spectral resolution of 4 cm^{-1} and 128 scans. Interpretation of the spectra was based on published data and the IRUG database.

Variable pressure-scanning electron microscopy coupled with energy-dispersive X-ray spectroscopy (VP-SEM/EDS)

A variable pressure Hitachi™ S-3700N SEM (Hitachi High-Tech® Europe GmbH, Germany) coupled with a Bruker™ XFlash 5010 SDD EDS® spectrometer (Massachusetts) was used for the analyses. The resolution of the EDS detector is 123 eV at the Mn Kα energy line. The samples were placed on a thin conductive carbon tape and analysed under a pressure of 40 Pa. Chemical analyses and imaging in the backscattered mode (BSE) were done with an accelerating voltage of 20 kV. Semi-quantitative data on elemental composition were obtained using Esprit1.9® software.

Pyrolysis–Gas chromatography coupled with mass spectrometry (Py-GC–MS)

A Frontier Lab PY-3030D (Frontier Laboratories Ltd, Japan) double-shot pyrolyser system was utilised, with the interface maintained at 280 °C. This pyrolyser was coupled to a Shimadzu GC2010 (Shimadzu Corp., Japan) gas chromatograph, which in turn connected to a GCMS-QP2010 Plus mass spectrometer. For separation, a Phenomenex Zebron ZB-5HT capillary column (30 m length, 0.25 mm internal diameter, 0.50 μm film thickness) was employed, using helium as the carrier gas at a flow rate of 1.5 mL/min. The split injector operated at a 15:1 ratio and a temperature of 250 °C. The GC temperature programme was as follows: starting at an initial temperature of 35 °C with a 1-min hold; it was then increased to 110 °C at a rate of 60 °C/min, followed by a rise to 240 °C at 14 °C/min, and finally up to 280 °C at 6 °C/min. The temperature was then raised to 320 °C at a rate of 30 °C/min, with a final hold time of 6 min. The ion source temperature was fixed to 240 °C, and the interface temperature was kept at 280 °C. The mass spectrometer acquired data across a range of 40–1090 m/z. Each sample (less than 200 μg) was placed in a 50 μL Eco-cup capsule and pre-derivatised using 3 μL of tetramethylammonium hydroxide (TMAH, 2.5% in MeOH). The derivatised samples were afterwards pyrolysed at 500 °C. For further details on the derivatisation procedure using tetramethylammonium hydroxide (TMAH), please refer to the following Application Note [26].

Compound and material identification was conducted using AMDIS software, integrated with the NIST20 and Wiley7 databases (match factor > 700), together with the Expert System for Characterisation using AMDIS Plus Excel (ESCAPE). ESCAPE is a semi-automated tool developed by the Getty Conservation Institute (GCI), which integrates the Automated Mass Spectral Deconvolution and Identification System (AMDIS) with a custom Excel workbook. This approach significantly enhances the efficiency and accuracy of identifying organic materials in complex mixtures.

The process begins with AMDIS deconvoluting the complex mass spectral data from the Py-GC–MS analysis, isolating individual component spectra, and comparing them to a customised marker compound library. This library, which contains over 1600 entries compiled from reference materials and scientific publications, includes markers for proteins, lipids, carbohydrates, resins, and other materials commonly encountered in cultural heritage research [27, 28].

Once the AMDIS report is generated, the ESCAPE workbook is used to import and organise the data into tables categorised by material classes. For protein identification, specific marker compounds—molecules formed from the pyrolysis of polypeptides in the presence of TMAH—are evaluated. ESCAPE provides tools such as bar graphs and pie charts that visually summarise the data, allowing users to confirm the presence of materials by cross-referencing marker compounds with expert knowledge embedded in the workbook. These tools help ensure that data interpretation remains consistent and reproducible, even for users with limited experience in Py-GC–MS [29].

Natural dyes extraction

Dyed wool samples (around 2.0 mg) were placed in vials, and 1.0 mL of a 0.1% EDTA solution in a 1:1 (v/v) mixture of water and DMF was added. The vials were fastened and heated at 100 °C for 30 min. After this, the solvent was removed via freeze-drying. Dried samples (excluding blue/green colours) were re-dissolved in 250 μL of a 1:1 (v/v) solution of MeOH and H_2O, while blue/green samples were re-dissolved in 250 μL of a 1:1 (v/v) solution of MeOH and DMF. Following re-dissolution, all samples were filtered through a 0.45 μm PTFE filter before the HPLC analysis.

High-performance liquid chromatography with diode array and mass spectrometry detection (HPLC–DAD-MS)

A Thermo Finnigan LCQ Fleet (©Thermo Fisher Scientific Inc., Massachusetts) mass spectrometer, equipped with an ESI source, an ion trap mass analyser, and a PDA detector, was employed for the analyses. The MS analysis conditions included a capillary temperature of 300 °C, source voltage of 5.0 kV, source current of 100.0 μA, and capillary voltage of − 3.0 V in negative ion mode and 22.0 V in positive ion mode. Analytes were detected in full MS mode (m/z 100–800). For negative ion mode, two source-induced dissociation (SID) segments were applied: 10.0 V SID from 0 to 12 min and 30.0 V CID from 12 to 30 min; for positive ion mode, 30.0 V SID was employed from 0 to 30 min. The column and tray temperatures were maintained at 30 °C and 24 °C, respectively. The DAD detector operated within the range of 200–800 nm. The MS and DAD instruments were coupled to an LC system featuring a Surveyor Thermo Finnigan autosampler. The analytical column used was a reversed-phase Agilent Zorbax Eclipse XDB-C18 (C18, 3.5 μm particle size, 150 × 2.1 mm; Agilent Technologies). The mobile phase consisted of acetonitrile (A) and water acidified with 0.1% formic acid (B). The gradient elution was set to 0–63% A from 0 to 14 min, followed by 63–90% A from 14 to 25 min, and 90% A from 25 to 30 min. The mobile phase flow rate was 0.2 mL/min, and the injection volume was 20 μL.

3 Results and discussion

3.1 Unearthing the *simulacra*'s context and location

In Fig. 1, the *simulacra* of St. Theodore and St. Primogenita are displayed. Both individuals rest on a mattress with two cushions, each positioned differently, reflecting the variations in body arrangements observed in other analysed *simulacra* [30]. St. Theodore lies in eternal rest, in the supine position, with the trunk twisted to the left, facing the observer. St. Primogenita's position is less distinct due to degradation of the face and cranium; however, the head was likely elevated, resting on the right hand, with the elbow supporting the body and the trunk twisted to the right, facing the observer.

Little is known about how these child *simulacra* arrived in Portugal, including who commissioned them and the reasons behind the order. It remains uncertain whether they were indeed martyrs or if they came to Portugal together. The historical research conducted so far has revealed that there is a tradition suggesting Pope Pius IV (1559–1565) gifted relics of saints to Lourenço Pires de Távora (1510–1573), who served as Portugal's ambassador to the papacy upon his return to the Kingdom in 1562 [31]. This nobleman preserved them at his estate in Caparica. However, there is no evidence to confirm that these were precisely the same relics, mainly because both Lourenço Pires de Távora and the Pope lived before the discovery of the Roman catacombs. In the nineteenth century, the relics were housed in the Chapel of Nossa Senhora do Bom Jesus, adjoining the manor of the Lords of Caparica. In the latter half of the century, when the 3rd Count of Caparica sold the manor, he entrusted the relics to Santa Casa da Misericórdia de Almada (SCMA), a social welfare institution, through the manor's administrator, who had previously served as the Provider for the Misericórdia in 1831 and 1832 [31].

The Hospital of Misericórdia de Almada operated from 1947 to 1991, during which its annexed church was converted into a mortuary chapel and morgue. As the hospital expanded, the church's side chapels were dismantled, and an additional floor was constructed above the church roof. The Santa Casa da Misericórdia de Almada collection features a mother and child, two other adults, and three children. In the archaeological campaigns of 1981 and 1982, the two adults and the mother and child were relocated to the attic of the Santa Bárbara estate, while one child remained in the church. Photographic records from that period, prior to the move of the *simulacra*, show these individuals positioned in the church's nave, except for St. Theodore and St. Primogenita. It is possible that during this time, the urns of St. Theodore and St. Primogenita may have been placed behind the altarpiece in a pit that served as a dumping ground for building materials (Fig. SI1), meaning they were never in the nave. In 2012, during the church rehabilitation, the small urns were found in that location, broken and covered in debris. After a brief cleaning, they were moved to the attic, where the other *simulacra* were already stored. The urns of St. Theodore and St. Primogenita likely originated from destroyed side chapels prior to the 1980s, explaining their absence during the 1981 and 1982 transport.

The urn of St. Theodore contained a paper cartouche (sample T3) inscribed with the Latin phrase, translated as: "True body of St. Theodore, young martyr, from the cemetery of Callixtus" (Fig. SI2a). In the case of St. Primogenita, no paper cartouche was found, probably due to the destruction of the urn. A General Inventory of the Church of Misericórdia de Almada, dated 31 December 1948, described the set of relics as mummy relics, likely based on direct or indirect consultation of the *authentica* documents or other now-lost records, a description that echoed in the 1949 inventory. St. Primogenita's name appears in this inventory, and the name association with this individual was established through a process of elimination. The inventory also noted that both St. Theodore and St. Primogenita originated from the Catacombs of St. Callixtus [32].

Notably, St. Primogenita's urn bore an important temporal marker: a red wax seal with an imprint of a coat of arms from the Bishop who authenticated the relic and authorised its transportation to Portugal (Fig. SI2b,c). By comparing this seal with others found in the *authentica* documents in an unnumbered archival packet at the Historical Archive of the Patriarchate of Lisbon (referring to a bundle of relics originating from the Monastery of São Vicente de Fora), it was identified as the seal of Nicola Angelo Maria Landini, Bishop of Porphyreon (1764–1782). This identification was crucial for estimating the date of the relic's arrival in Portugal. Landini, a Hermit of Saint Augustine and Assistant to the Pontifical Throne, served as Prefect of the Sacred Apostolic Church and is known to have authenticated other relics during this period [33]. Thus, it appears that this operation took place in the second half of the eighteenth century, likely between 1770 and 1782. This timeframe aligns with the severance of diplomatic relations between the Holy See and Portugal from 1760 to the brink of 1770.

The critical condition of St. Primogenita has provided valuable insights into its handling and enabled the extraction of a cranium fragment for dating purposes. Radiocarbon dating supplied an additional crucial piece of information, indicating that the bone fragment was dated to 1771 ± 30 years BP. (Before the present, the results are given in years before 1950.) Calibration using OxCal [34], with a 2-sigma range and a 95.4% probability, yielded a calibrated age range (calibrated Anno Domini (cal AD)) of 219–365 cal AD. The 68.3% probability range was 261–339 cal AD. This period was marked by notable hostility towards Christians, particularly during Marcus Aurelius' government (161–180 AD), when anti-Christian literature began to proliferate, and informants faced less resistance, leading to widespread persecutions across various regions. In 202 AD, Emperor Septimus Severus (193–211 AD) issued an edict prohibiting further conversions to Judaism and Christianity, resulting in intensified persecutions, especially in North Africa and Egypt. Later, two major persecutions occurred: the first under Emperor Decius (249–251), who initiated Empire-wide persecution of Christians with notable intensity, and the second under Diocletian (284–305), who led the Great Persecution, widely regarded as the most severe attempt to eradicate Christianity entirely [35].

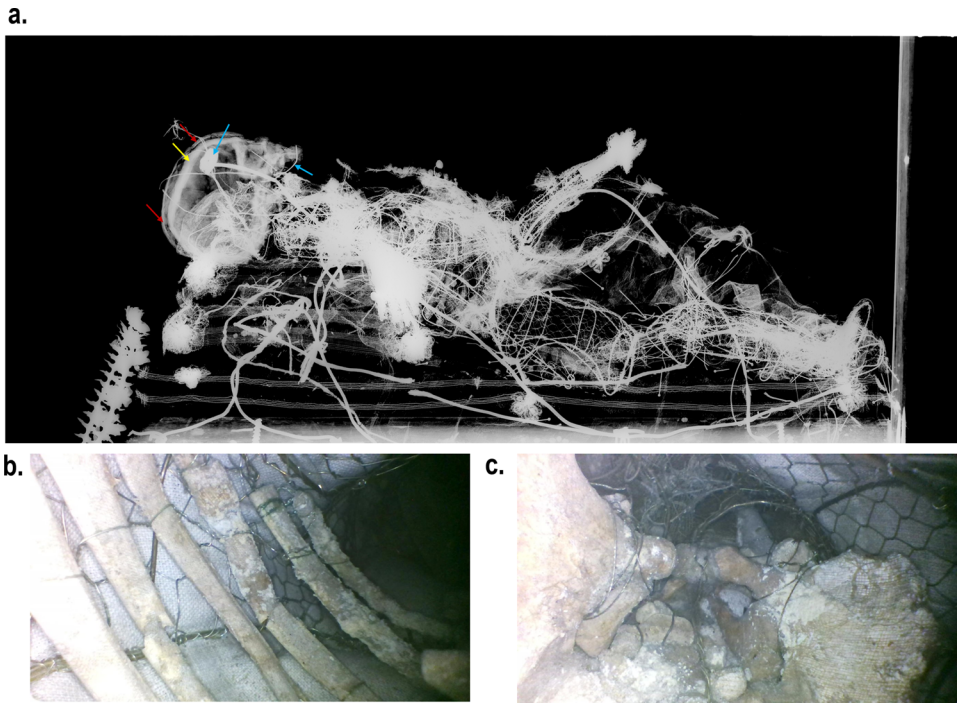

Fig. 2 **a** Radiographic imaging of St. Theodore *simulacrum*, with arrows indicating specific aspects discussed in the text; **b** and **c** borescope imaging revealed some bones and the internal structure used for securing the bones and shaping the body of St. Theodore

3.2 Deconstructing the *simulacra* assemblage: skeleton and materials

St. Theodore

In Fig. 2, a metal structure linking and supporting the bones is visible, surrounded by a metal net that gives the body's shape. The ribs are connected by twisted wire loops, forming an anatomically correct rib cage (Fig. 2b). The vertebrae were kept together by a larger cable extending from within the cranium (Fig. 2a, blue arrows), while thinner wires link each vertebra. The bones of the coxae—ilium, ischium, and pubis—are separated as expected for very young children, as these bones typically fuse after 11 years of age [36]. At their meeting point, the three bones are joined by a white substance (Fig. 2c), whereas a darker substance connects the coxae to each other (pubic symphysis) (Fig. 2c). Wires also secured these bones and the vertebrae from the sacrum. Notably, the length of the right ulna (approximately 7 cm) indicates this individual died at approximately six months of age [37]. Radiographic imaging also reveals a few indistinct teeth. It appears that the mandible does not belong to the same individual as the maxilla; the development of the upper teeth suggests an age at death between 4.5 and 7.5 months, while the lower teeth indicate an age of approximately 2.5 years [38]. Additionally, the bones of the hand and foot are slightly displaced but correctly positioned, with the phalanges of the left hand partly covered or supported by fabric. A wire is wrapped around the radius and its epiphysis in the left hand. The wrist area contains several epiphyses resembling carpal bones, but the phalanges seem properly positioned and appropriately sized compared with the rest of the skeleton (Fig. 2a).

This skeleton is notably complete and exhibits signs of preparation by someone with advanced knowledge of human anatomy, particularly given the young age of the individual.

The fabric covering St. Theodore's head does not allow direct observation of the cranial bones. However, the radiography (Fig. 2a) reveals that the cranium (red arrows) was reconstructed atop a metal structure (yellow arrow) designed to mimic its shape. Additionally, metal rods go inside the cranium to keep it in the correct anatomical position, while another structure supports the mandible (blue arrows). The facial structure features three layers of silk gauze on the outermost surface, followed by a middle layer of cotton fibres to add volume and texture, with the cranium serving as the base. BFM observations of samples T27, T28 (silk gauze), and T31 (cotton) confirmed the nature of these fibres (Fig. SI3a). The layers of silk gauze were sewn together to a gauze covering and supporting the back of the cranium (occipital bone), significantly fragmented, and secured in place by a half-mooned metallic wire (Fig. SI4a). The occipital bone has residues on the ectocranium surface, possibly of lime deposits from the decomposition site. No biomarkers were detected in the Py-GC–MS analysis of sample T30, a residue from St. Theodore's ectocranium. While the sample size is small and might lack representativity, this result suggests a distinct procedure used in the cranium consolidation of St. Theodore compared to that of St. Primogenita.

The silk fibres consist mainly of fibroin and sericin proteins, the latter acting as a protective coating for fibroin. Sericin forms a hydrophilic, glue-like matrix around silk fibroin, enhancing the fibre's structure and contributing to its hardness. The process of removing sericin, known as degumming, is commonly employed in silk manufacturing to yield a softer fibre with improved lustre and texture, suitable for textile production [39, 40]. This process typically results in a weight loss of about 25%, often compensated

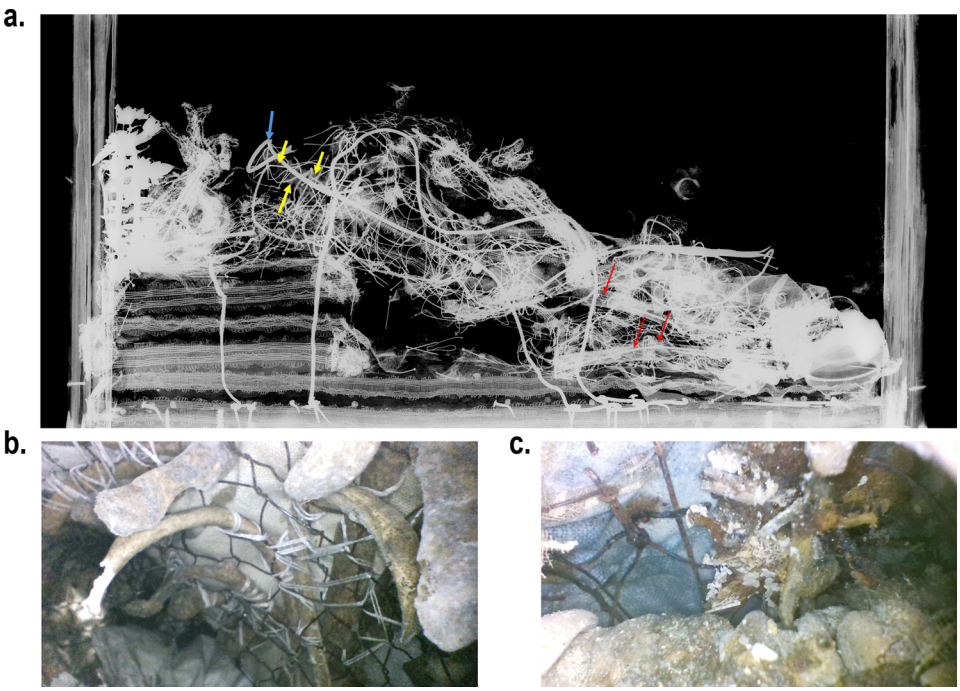

Fig. 3 **a** Radiographic imaging of the St. Primogenita *simulacrum*, with arrows highlighting specific features discussed in the text; **b** borescope imaging illustrating the rib assemblage method used for St. Primogenita, in contrast to St. Theodore's (Fig. 2b); **c** a white substance was used to secure the vertebrae, similar to the treatment observed in the os coxae of St. Theodore (Fig. 2c)

for inorganic salts [39–41]. The FT-IR spectrum of the silk gauze, sample T4 (Fig. SI4b), showed distinct bands characteristic of silk materials, including 3385 and 3069 cm^{-1} (νNH) for amide A and B, as well as 1624 cm^{-1} (C=O), 1505 cm^{-1} (δNH and νCN), and 1224 cm^{-1} (δNH and νCN) for amide I, II, and III, respectively [39, 41]. Additional insights into sericin presence were gathered, with literature [39, 42] indicating that sericin is primarily identified by a fingerprint marker at *ca.* 1380–1420 cm^{-1} (δCH_3, δCOH, νCO, polyalanine glycine (Ag), serine (Ser)), along with bands at *ca.* 1058–1030 cm^{-1} (νCO, Ser), and 980 cm^{-1} (νCC, νCO, Ser). While νCO, Ser vibrations were detected (~ 1030 cm^{-1}), the band's intensity at *ca.* 1405 cm^{-1} was very low, and the band at 980 cm^{-1} was absent, suggesting residual sericin, indicating that the raw silk was likely degummed as often occurred for high-quality textiles. Furthermore, the absence of a feature at ~ 965 cm^{-1} may suggest that the silk is derived from *Bombyx mori*, as this feature, attributed to the alanine-alanine (Ala-Ala) peptide structure, is characteristic of species like *Antheraea pernyi* but often absent in *Bombyx mori* [43]. Additionally, the extensive use of *Bombyx mori*-derived silk in Europe is well-documented, establishing it as a primary material in European textile traditions [44, 45].

FT-IR analysis also revealed inorganic salts, such as calcium and oxalate salts. Bands indicative of calcium carbonate were observed at 1430 cm^{-1} ($\nu_{3\,s}(CO_3^{2-})$), 876 cm^{-1} ($\nu_{2\,as}(CO_3^{2-})$), and 718 cm^{-1} (($\nu_{4\,s}(CO_3^{2-})$), alongside calcium sulphate at 3533 cm^{-1} (νOH), 1108 cm^{-1} ($\nu_{3\,as}(SO_4^{2-})$), 919 cm^{-1} ($\nu_{1\,s}(SO_4^{2-})$), and 606 cm^{-1} ($\nu_{4\,as}(SO_4^{2-})$) [46, 47]. Calcium oxalate was also identified through features at 1327 cm^{-1} ($\nu_s OCO^-$) and 790 cm^{-1} (δOCO^-). This last compound is typically a minor component in silk, likely resulting from the excretion of the silkworm after feeding on oxalic acid-rich leaves [39, 48]. The low intensity of the IR features suggests only minute amounts of calcium oxalate.

The silk gauze is stiffened to shape the face, likely formed over a mould. The Py-GC–MS analysis (Fig. SI5) identified a few non-specific protein markers in the solid residue extracted from sample T4 (Table 1), suggesting the use of a proteinaceous substance in the sculpting process of the face; however, the material's origin remained inconclusive. The calcium salts may have also been used as fillers in this proteinaceous substance, likely an adhesive, creating a more substantial and voluminous, sculpted foundation for the face.

St. Primogenita

The radiographic imaging of St. Primogenita (Fig. 3a) showed that the mandible and teeth are absent, potentially lost due to the significant damage to the *simulacrum*. The fused metopic suture suggests an age at death older than two years [36], while the length of the humerus may indicate an age at death of less than one year [37]. This discrepancy in age estimates raises the possibility that the bones may not belong to the same individual or that the individual experienced a growth delay of *ca.* one year.

At the top of the *simulacrum* structure, a large loop on the metal rod (Fig. 3a, blue arrow) appears to be intended to support the head, with several vertebrae visible along its length (Fig. 3a, yellow arrows). The left forearm seems to contain a paste, where the bones (radius and ulna) may be embedded or absent, suggesting a later modification as the forearm's netting is open. In contrast, the right forearm retains both the radius and ulna, with at least one bone pierced by wire. The phalanges are also wired longitudinally to form the fingers, with a curved wire end visible in one digit (Fig. 3a). A metallic net shapes the body, with ribs intertwined and sewn into the netting (Fig. 3b). The vertebrae are seemingly held together with a paste (Fig. 3c). Although the radiographs are limited

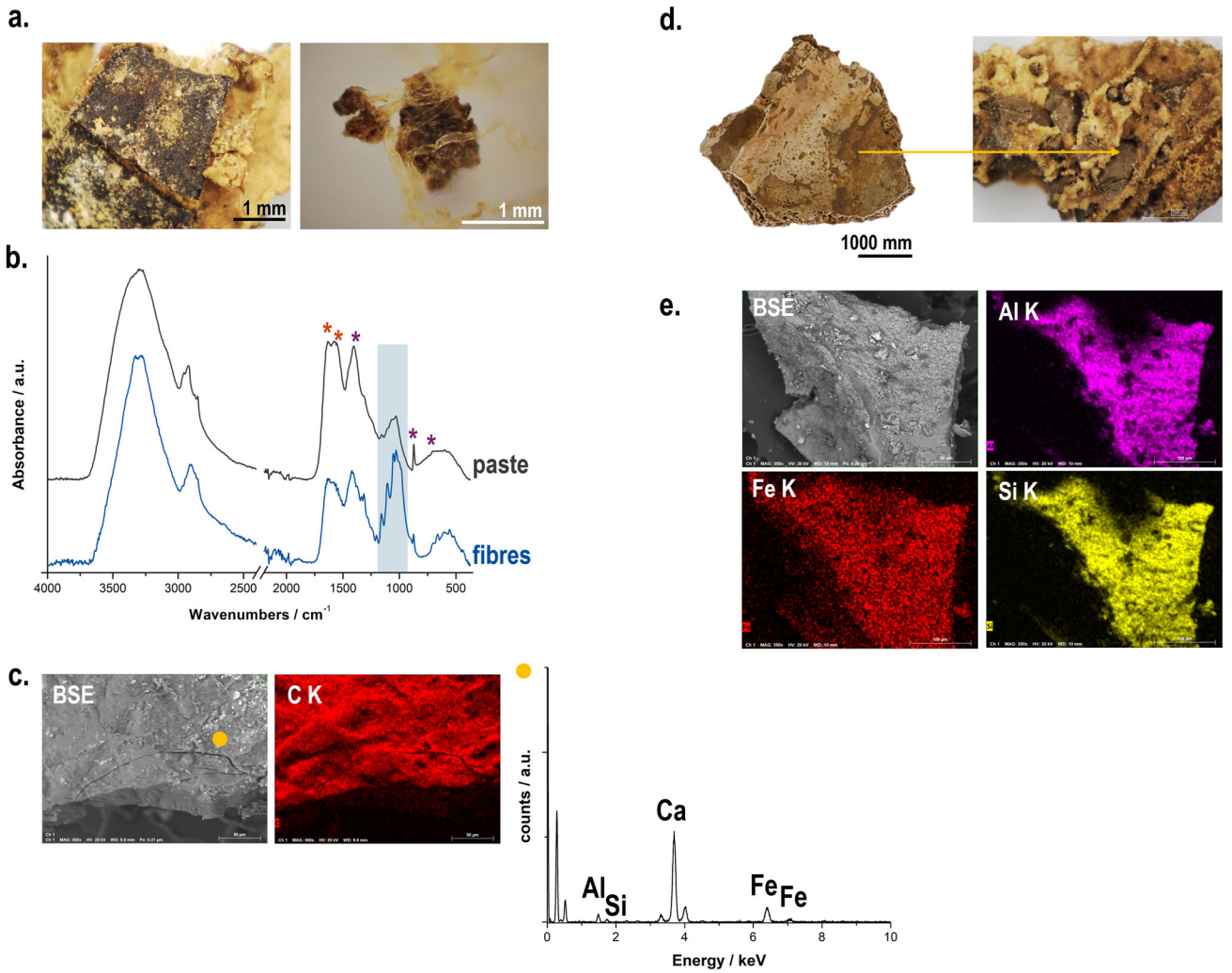

Fig. 4 **a** microscopic image of sample P38, a bone fragment showing the ectocranium lined with a fibrous material covered with a dark brown paste; **b** FT-IR spectra of the dark paste and fibres, with the cellulose fingerprint region highlighted by a blue vertical strip, and the key bands of a proteinaceous material and calcium carbonate indicated in orange and purple asterisks, respectively; **c** BSE micrograph and C elemental map of the dark paste, with the corresponding EDS spectrum showing the presence of Ca and Fe; **d** photograph of a cranium fragment and respective microscopic image, displaying a cement-like material in the endocranium (sample P39) and the Al, Si, and Fe elemental distribution maps

due to the bones being less dense than the surrounding metal structure and the substantial amounts of metal in both the frame and the textiles, broken leg bones, including the femora and tibiae, are observable (Fig. 3a, red arrows).

The cranium of St. Primogenita is fractured, and the facial structure is severely damaged, with the remaining layers of gauze losing their original shape (Fig. 1). BFM observations of a gauze sample from the chest (samples P33 and P34) confirmed the silk nature (Fig. SI3b). Sample P38 comprises a fibrous material coated with a dark brown paste, likely used to line and bond the unfused parts of the cranium (Fig. 4a).

FT-IR analysis of this fibrous material of sample P38 confirmed it to be cellulose-based, likely from paper, as evidenced by the characteristic fingerprint region indicated in the blue strip (Fig. 4b and Table SI1). BFM observations showed the presence of bast fibres (Fig. SI3c). The Py-GC–MS analysis provided additional insights by revealing that several non-specific and specific protein markers, pyrrole, and indole derivatives were detected. These markers are characteristic of pyrolysis products of amino acids such as proline, hydroxyproline, and tryptophan, which are abundant in collagen [49] (Fig. SI6a). Their presence strongly suggests the use of animal glue in this material, consistent with its historical use for structural repairs or adhesion [27].

As to the dark brown paste, the FT-IR spectrum shows amide features (1632 cm^{-1} (C=O) and 1561 cm^{-1} δNH and νCN) (Fig. 4b, orange asterisk), suggesting the presence of proteinaceous material. The Py-GC–MS data (Fig. SI6b) revealed a pattern of protein markers, including pyrrole and indole derivatives, alongside the detection of long-chain saturated fatty acids (primarily palmitic (C16:0) and stearic (C18:0) acids (with a palmitic/stearic ratio exceeding 3) and cholesterol. Cholesterol is a key lipid component of egg yolk, a historically used binder or coating due to its adhesive and film-forming properties [27, 28]. Furthermore, the absence of

Table 2 Summary of textile descriptions for the various items in St. Theodore and St. Primogenita

Item	St. Theodore	St. Primogenita
Mantle	Pattern with strips meandering colourful floral bouquets and fur (silk and metal threads) on a violet ribbed ground	Blue satin ground with meandering floral motifs (silk and metal threads)
Dress	Meandering pattern with peacock feathers between baskets of flowers on metallic ground; The peacock feathers are typical of the fashion taste in the second half of the eighteenth century	Carmine satin
Skirt (under the dress)	–	Colourful floral motifs on a metallic ground
Sleeves (with another fabric)	Colourful floral motifs on a metallic ground	–
Carnation	White gauze	White gauze
Two cushions	Blue silk satin	Beige silk satin
Mattress	Carmin silk satin	Blue-striped ground with yellow floral bouquets
Braids	(7 types) Braid of silk and silver-gilt threads woven in a simple geometric pattern; most have picot-edged effects	(6 types) Braid of silk and silver-gilt threads woven in a simple geometric pattern; most have picot-edged effects
Lace	Gilt bobbin lace with shell motif; Border lace to adorn/finish the hem, neckline and sleeves of the costume; Highlight the symbolic shell motif	Gilt bobbin lace with shell motif; border lace to adorn/finish the hems, neckline and sleeves of the costume; highlight the symbolic shell motif
Lace	White silk (?) bobbin lace with shell motif	White silk (?) bobbin lace with shell motif

squalene, a major, oxidation-prone constituent of human skin lipids, strongly argues against recent contamination [50]. Collectively, these data support the interpretation that an egg-based material was employed in the sample composition. Calcium carbonate was also detected through the vibrational modes of carbonate (1410 and 872, 720 cm^{-1}) [51], and EDS analysis revealed a significant presence of Ca-rich particles unevenly distributed across the sample's surface (Fig. 4c). A limited presence of Ca- and S-rich particles was also observed. Since Ca particles were predominantly located on the surface, it seems that calcium salts were not deliberately added as fillers for the organic matrix; rather, they likely formed due to environmental exposure, with the cranium serving as the main calcium source. EDS point analysis suggests that hematite may have been added to the organic matrix, contributing to the dark brown hue (Fig. 4c).

The endocranium appeared to be reinforced with a light brown material (sample P39) (Fig. 4d) that filled the porous bone structure, providing cement-like properties that likely enhanced the structural stability of the cranium in this very young individual. EDS analysis showed a predominance of Al, Si, and Fe (Fig. 4e), suggesting an inorganic composition. Currently, there is limited information on iron-aluminosilicate consolidants used in bones. Laterite, a clayey material primarily composed of kaolinite, is often found in tropical and subtropical regions and is commonly used in consolidation in civil construction [52]. A similar consolidating material may have been used in the endocranium of St. Primogenita. Py-GC–MS analysis provided information on organic compounds within the inorganic matrix, including several non-specific and specific protein markers (mainly pyrrole derivatives), which are related to the pyrolysis of collagen (Fig. SI6c). This evidence supports the conclusion that animal glue was possibly the proteinaceous material in this sample. Unlike the dark brown paste in sample P38, no cholesterol or other relevant lipid markers were detected, further corroborating that the material in P39 was very likely an animal glue [27].

3.3 Unveiling the textiles

A comparison of the two *simulacra* regarding their garments, mattresses, and cushions revealed both similarities and differences, summarised in Table 2. Both *simulacra* feature a mantle and a dress, though St. Primogenita additionally includes a skirt beneath the dress.

The figured fabrics used in both *simulacra* present a meandering compositional structure where the design is marked by sinuous vertical lines, either parallel to each other or opposing, where whatever motif is represented—floral, plumage, lace, and galloons—must be subordinate. These characteristics reflect eighteenth-century tastes and fashions in French textile manufacturing.

Natural dye identification in thirty-seven representative textile threads, comprising wefts, warps, and core silk threads from both *simulacra*, was conducted using LC-DAD-MS to unveil the natural products used for dyeing. To complement the findings on thread colouration, SEM–EDS analysis was performed on most samples for mordant identification (Table 3). Alum ($KAl(SO_4)_2.12H_2O$) has traditionally been the most common mordant for red and yellow flavonoid dyes, noted for the brilliance of the dyed threads. In contrast, iron salts, such as iron sulphate ($FeSO_4.7H_2O$), are often associated with significantly dark hues [53, 54]. Yellow and green threads were primarily characterised by weld chromophores, mainly luteolin derivatives, alongside a few apigenin-derived compounds and indigotin in green threads. This combination of weld and indigo/woad reflects a historical method for achieving green shades [55]. A quercetin glucoside detected in one yellow sample (P8) indicates a different flavonoid dye source, as weld typically features luteolin and apigenin as major constituents along with their *O*-glucoside derivatives [56]. Aluminium was identified as a mordant in these yellow and green samples, aligning with its historical use to produce vibrant yellow colours [55]. Two dark brown samples (T15, T23) also revealed yellow flavonoid chromophores. The presence of iron mordant, associated with darker shades [53], explains the colouration of sample T23. For sample T15, while the mordant could not be determined, the presence of three luteolin-based compounds suggests weld was used. In sample T23, a quercetin derivative was identified, excluding the use of weld dye and leading to the proposal of an alternative flavonoid dye source. In red/pink samples T23a and P6, carminic acid and the α/β C-glucofuranosides of kermesic acid, dcIV and dcVII, were identified, both mordanted with aluminium salts. These chromophores are characteristic of a cochineal dye, likely of American origin, given the chronology and the absence of characteristic minor compounds of Armenian and Polish cochineal dyes. Among pink/orange/yellow threads, only chromophore urolithin C, a marker for red brazilwood dye, was detected [57], with Al as the mordant. Indigotin was detected in several blue samples as a single component, indicating indigo or woad as the primary blue dye source. In blue sample P23, an additional chromophore, urolithin C, was detected, suggesting the use of both indigo or woad and brazilwood to achieve a purple hue.

The absence of detectable chromophores in six coloured samples indicates that the extraction process was ineffective, and any degradation of dye compounds did not yield quantities above the instrument's detection limits. The other three white samples with no chromophores detected, T18a, T20, and T29, likely underwent no dyeing procedure. As to mordants, it was not possible to estimate their use in several yellow, green, and pink/red colours. However, no mordant was expected for indigo, as it is a vat dye that does not require a mordant in the dyeing process [53].

Metal threads were extensively used in the garments of the *simulacra*. Figure SI7 illustrates different metal threads and their conservation state. Representative metal threads analysed are summarised in Table 4. Samples were primarily solid metal strips and strips wound around a fibrous silk core featuring S-twist (Fig. SI7b,c) and Z-twist (Fig. SI7e) metal coils. Based on Hacker et al. [58], the metal threads in this work were generally categorised as thin-diameter (200–250 μm) with two coils per unit length. Additionally, a larger diameter thread (>410 μm) with a similar coil distribution was found in St. Primogenita's metallic lace. Our results align with those reported by Tronner et al. [59], who noted no significant differences in the geometrical dimensions (thickness and width of the strip) of gilt silver threads from 1400 to 1900, with widths around 200–600 μm and thicknesses of 10–50 μm.

The edge morphology and the gilding layer are key features in uncovering the manufacturing techniques in metal strip production. Features such as smooth, rounded edges, striation from the drawing process in which metal strips are pulled through a drawplate before flattening, and double-sided gilt layers indicate a "cast, drawn, and rolled" production technique [58, 60]. Striations are clearly observable on the metal gilt strips using BSE imaging due to the density difference between the gold layer and the silver or the silver–copper strips [60, 61]. SEM–EDS and optical microscopy confirmed rounded edges (Fig. 5a-c), longitudinal striations (Fig. 5d–f), and double-sided gilt strips, suggesting production pos-late 15th or the sixteenth century, when the "cast, drawn, and rolled" technique was introduced [58, 61].

SEM–EDS was also employed to analyse the cross sections of all metal strips for bulk composition estimation. All threads were made of silver and copper with a high Ag content between 100–98 wt% and a 0–2 wt% Cu content, whether gilt or not, indicating the use of high-quality materials [62]. These results align with findings by Bergstrand et al. [63], who studied seventeenth- and eighteenth-century Swedish ecclesiastical metal embroidery. Hacke et al. [64] noted that silver metal threads produced in Italy and England during the seventeenth–eighteenth centuries typically contained ~ 2–5% Cu and ~ 0–6% Au in the silver bulk.

Metal thread degradation may result from manufacturing processes, handling, improper storage, or, most critically, corrosion, the main cause of decay in metal strips [60, 61, 64]. Figure SI8 shows an EDS analysis of representative samples indicating the presence of Cl and S, suggesting the formation of chloride- and sulphide-based silver corrosion compounds. These compounds were found in all metal threads from both *simulacra* and were attributed to exposure to fluctuating atmospheric conditions, such as temperature and humidity. Inadequate storage has probably exacerbated these conditions. No copper corrosion compounds were detected, likely due to the high silver content, although their presence remains possible. Corrosion typically develops along striation lines, scratches, and pits [58, 60], exposing more the silver–copper alloy in these areas. SEM micrographs of representative silver corrosion morphologies are presented in Fig. SI8, showcasing elongated silver sulphide crystals, leaf-shaped chloride crystals, and evident delamination and cracking.

3.4 Symbols of martyrdom and decorative elements

St. Primogenita was the only *simulacrum* to feature the phial of blood (sample P40). Figure 6 shows both the external and internal surfaces of the glass fragment, highlighting the associated degradation. Pitting and crizzling, likely caused by prolonged exposure

Table 3 HPLC–DAD-MS identification of natural dyes and EDS information on the mordants in samples collected from the garments and accessories of St. Theodore and St. Primogenita

Sample |colour	Retention time (min.)	λ máx (nm)	$[M–H]^-$ (m/z)	Peak identification	Possible dye source	Mordant
T2 | green T12 | green T13 | green	16.04	335	609, 447, 285	Luteolin-di-O-glucoside	Weld + indigo or woad	Alum (Al)
	16.75	345	447, 285	Luteolin-7-O-glucoside		
	19.41	347	285, 151, 133	Luteolin		
	20.50	332	269, 151, 117	Apigenin		
	23.95	607	263, 219 (positive mode)	Indigotin		
T8 | yellow T18a | white T20 | white T29 | white P1 | red P11 | light blue P16 | light blue P35 | yellow P21 | green	–	–	–	–	No chromophore detected	–
T10 | pink T11 | pink T14 | orange T17 | orange T18 | red P5 | yellow P25 | pink	20.10	332	243, 187	Urolithin C	Brazilwood	Alum (Al) (T11 & T17, below detection limit)
T15 | brown	16.04	335	609, 447, 285	Luteolin-di-O-glucoside	Possibly weld	–
	16.75	345	447, 285	Luteolin-7-O-glucoside		
	19.41	347	285, 151, 133	Luteolin		
T16 | blue P7A | blue P7V | blue P22 | blue	23.95	607	263, 219 (positive mode)	Indigotin	Indigo or woad	–

Table 3 continued

Sample |colour	Retention time (min.)	λ máx (nm)	$[M–H]^-$ (m/z)	Peak identification	Possible dye source	Mordant
T21 | green	16.04	335	609, 447, 285	Luteolin-di-O-glucoside	Weld + indigo or woad	Alum (Al)
	16.75	345	447, 285	Luteolin-7-O-glucoside		
	17.66	340	447, 431, 285, 269	Luteolin-O-glucoside + apigenin-O-glucoside		
	19.41	347	285, 151, 133	Luteolin		
	20.50	332	269, 151, 117	Apigenin		
	23.95	607	263, 219	Indigotin		
T22 | yellow T26 | yellow	16.04	335	609, 447, 285	Luteolin-di-O-glucoside	Weld	Alum (Al)
	16.75	345	447, 285	Luteolin-7-O-glucoside		
	19.41	347	285, 151, 133	Luteolin		
	20.50	332	269, 151, 117	Apigenin		
T23 | brown	16.58	370	463, 301	Quercetin-glucoside	Flavonoid dye source	Iron sulphate (Fe)
	16.75	345	447, 285	Luteolin-7-O-glucoside		
T23a | red P6 | pink	15.58	490	491, 447, 357, 327, 299	Carminic acid	Cochineal	Alum (Al)
	16.81	489	491, 447, 357, 327, 299	α-C-glucofuranoside of kermesic acid (dcIV)		
	17.12	492	491, 447, 357, 327, 299	β-C-glucofuranoside of kermesic acid (dcVII)		
T23b | yellow	16.04	335	609, 447, 285	Luteolin-di-O-glucoside	Weld	Alum (Al)
	16.75	345	447, 285	Luteolin-7-O-glucoside		
	17.66	340	447, 431, 285, 269	Luteolin-O-glucoside + apigenin-O-glucoside		
	19.41	347	285, 151, 133	Luteolin		
	20.50	332	269, 151, 117	Apigenin		
P8 | yellow	16.58	370	463, 301	Quercetin-glucoside	Flavonoid dye source	Alum (Al)
P10 | green P13 | green P15 | green P19 | green	16.04	335	609, 447, 285	Luteolin-di-O-glucoside	Possibly weld + indigo or woad	–
	16.75	345	447, 285	Luteolin-7-O-glucoside		
	19.41	347	285, 151, 133	Luteolin		
	23.95	607	263, 219 (positive mode)	Indigotin		
P23 | blue	20.10	332	243, 187	Urolithin C	Brazilwood + indigo or woad	–
	23.95	607	263, 219 (positive mode)	indigotin		

Table 4 Summary of the metal threads analysed, including metal strips width and thickness

	Sample ID	Item	Description	Metal strip	
				Width (μm)	Thickness (μm)
St. Theodore	T6	Mantle	Double-sided silver-gilt strip	215	40
	T8	Mantle	Double-sided silver-gilt strip wound around a silk core	220	12
	T18	Mantle	Silver strip wound around a silk core	250	17
	T19	Dress	Silver strip	280	18
	T20	Dress	Double-sided silver-gilt strip wound around a silk core	215	16
	T26	Dress sleeve (lace)	Double-sided silver-gilt strip	235	15
	T29	Glove	Silver strip wound around a silk core	213	19
St. Primogenita	P18	Mantle	Silver strip	300	24
	P19	Mantle	Double-sided silver-gilt strip wound around a silk core	190	14
	P29	Skirt	Double-sided silver-gilt strip wound around a silk core	225	14
	P31	Skirt	Silver strip	300	41
	P35	Dress hem	Double-sided silver-gilt strip	312	18
	P36	Dress hem	Double-sided silver-gilt strip	726	14

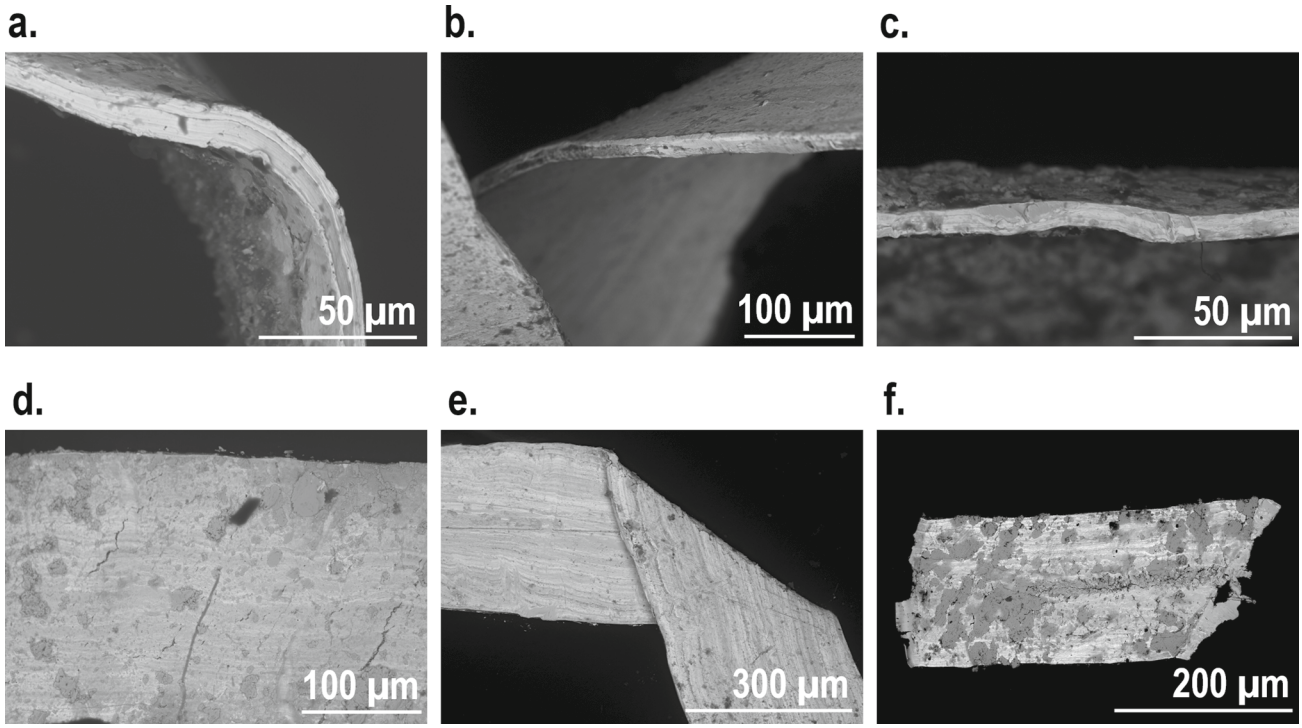

Fig. 5 **a–c** SEM micrographs illustrating the smooth and rounded edges (samples T6, P35, T20); **d–f** longitudinal striation lines due to the manufacturing process (samples T6 and P19)

to fluctuating humidity, were observed on the exterior (Fig. 6a–c). These alterations are reported as structural changes within the glass matrix, manifesting as pits and fine surface cracks over time [65]. Delamination was also noted. This degradation phenomenon can occur due to the dissolution of glass, which leads to the formation of a gel-like layer that dries and fractures into a network of cracks and flakes [65, 66].

The EDS analysis of the glass external surface revealed the presence of Si, K, Na, and Ca, suggesting that the phial is made from a mixed alkali-type glass. Figure 6d illustrates the glass interior, which features an amber-coloured layer with unevenly distributed black crusts. A brown residue of particle aggregates and fibres is also noted on this amber layer (Fig. 6d, e). This layer does not seem to take part in the glass composition. Further EDS analysis of the amber layer primarily identified Mn and Ca, with low amounts of Fe (data not shown). In contrast, the glass matrix showed no Mn and only residual Fe. Historical analysis conducted in the second half of the nineteenth century at the Greenwich Observatory examined about 60 phials of blood. It was found that a dark reddish

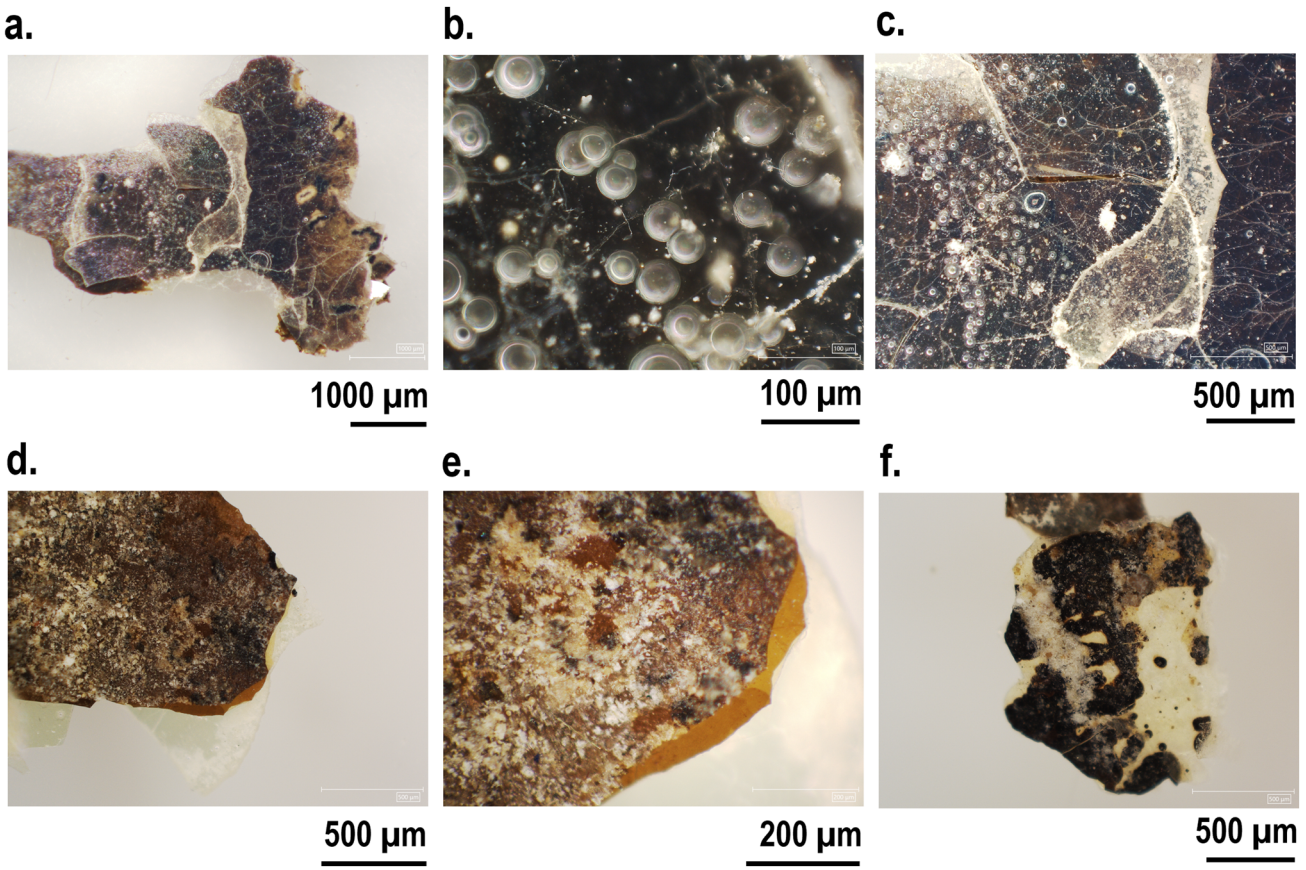

Fig. 6 **a–c** external surface of the phial of blood (sample P40) exhibiting degradation; **d**, **e** internal surface, where an amber-coloured layer is partially covered by a brown residue of particles and fibres; **f** black crusts are unevenly distributed in the internal surface

film sometimes appeared on the outside, inside, or between the layers of decomposed glass. This film, consisting entirely of Fe, was present in such quantities that it could not have originated from blood deposits. Instead, it was determined that the film of iron rust resulted from iron leaching from the glass itself [67]. With this context in mind, it is possible that the amber layer likely resulted from the intentional addition of Mn- and Fe-based compounds or suspensions of inorganic solids in water to simulate blood. Given the phial's intended function of preserving the martyr's blood, a task often deemed impossible, creative methods were likely employed to emphasise or achieve this goal.

Additionally, FT-IR analysis of the brown residue in contact with the amber layer revealed the presence of proteinaceous materials, fatty acids, and lipids (Table SI2). Py-GC–MS analysis detected some non-specific protein markers, though they were insufficient to determine the material's origins. While the possibility of some content of genuine blood being present in the phial cannot be entirely ruled out, if it existed, it would likely have been accentuated by a mixture prepared to simulate blood. The composition and appearance of the amber layer suggest that an additional colouring agent may have been added to deepen the colour, symbolically enhancing the representation of blood within the phial.

Another symbol of martyrdom is the flower crown, representing the imperishable crown of glory. The petals adorning the flower crowns of both *simulacra* were analysed (Fig. SI9). The FT-IR spectrum of St. Primogenita's crown (sample P1) displayed typical silk characteristics, dominated by amide features at 1617 cm^{-1} (C=O), 1514 cm^{-1} (δNH and νCN), and 1226 cm^{-1} (δNH and νCN)) [68]. Calcium carbonate was identified by its characteristic CO_3^{2-} vibration modes, likely serving as a filler material for the silk. Notably, this sample exhibited almost no red colour, with dye degradation obscuring the original hue. LC-DAD-MS analysis did not detect any chromophores (Table 3, sample P1), possibly due to an ineffective extraction process for remaining chromophores and degradation compounds, resulting in quantities below the instrument's detection limits. Additionally, Py-GC–MS analysis revealed some biomarkers indicative of proteinaceous material, primarily pyrrole derivatives and some indole-related compounds, suggesting the presence of animal glue. This adhesive may have been employed to bind the petals together, shaping each flower. In contrast, the petal from St. Theodore's crown (sample T2) consisted of a cellulosic-based material that appeared to have been coloured using a combination of pigment and dyes. Combined SEM–EDS and HPLC–DAD-MS analyses indicated a synergetic colouring method, incorporating a Cu-containing pigment (Fig. SI9b) along with weld and indigo or woad dyes (Table 3, sample T2).

The St. Theodore dress (Fig. 1) is embellished with beads at the neckline, armholes, and waist, while only a few beads remain in place on St. Primogenita's waist, and she still retains a beaded bracelet. Samples T1, T5, and P4 were analysed, revealing that they are primarily composed of gypsum coated with a wax-based material (Fig. SI10 and Table SI3). The FT-IR spectrum of this coating closely resembles that of beeswax, as documented in the literature [69, 70]. The lipid fingerprint of beeswax is often characterised by its *n*-alkane, saturated fatty acid, *n*-alcohols, and wax ester profile [71, 72]. Further insights were obtained by Py-GC–MS analysis (Fig. SI11), which confirmed the presence of biomarkers consistent with beeswax, aligning with the FT-IR results. Odd-numbered *n*-alkanes (C21 to C33, peaking at C27) and even-numbered fatty acids (C22 to C34), with lignoceric acid (C24) being the primary fatty acid, were detected [73]. Lignoceric acid is known to occur naturally in the propolis of *Apis mellifera,* the European honeybee found in Africa, Europe, and parts of Asia [74]. The detection of long-chain wax esters (C40) suggests that the material is well-preserved since hydrolysis typically affects the monoesters with shorter carbon chains [72]. Additionally, the presence of phenolic compounds offers insights into the conservation status of the waxes. Their limited presence, indicated by weak in-plane and out-of-plane bending of hydrogen atoms on the phenyl group [69] in the FT-IR spectrum (features in the 1220–950 cm^{-1} range and below 900 cm^{-1}), supports the assessment of a well-preserved material. Overall, no significant differences in composition or conservation state were found between the beads of the two *simulacra*.

4 Conclusions

This study presents the first comprehensive analytical approach to examining the *simulacra* of very young individuals exhumed from the Catacombs of Callixtus in Rome during the early modern period. The collected evidence suggests that these *simulacra* were likely sent to Portugal in the late eighteenth century, likely between 1770 and 1782. Key findings include the red wax seal on St. Primogenita's urn, which features the coat of arms of the Bishop of Porphyreon (1764–1782), serving as a temporal marker for the date of arrival in Portugal. Additionally, the characteristics of the fabrics align with eighteenth-century fashion, particularly the use of peacock feathers, popular in the latter half of that century. Radiocarbon dating, together with the red wax seal, confirmed that St. Primogenita originated from the early centuries of Christianity.

Examination of the *simulacra* revealed differences in assembly, suggesting that individuals with distinct expertise and anatomical knowledge crafted them. St. Theodore's assembly reflects anatomical precision and rigorous craftsmanship, while St. Primogenita's construction is less meticulous. Despite being in a deplorable state of conservation, access to St. Primogenita's cranium fragments allowed for identifying both organic and inorganic materials used to consolidate the cranium. Further research is needed to determine whether the *simulacra* were assembled locally in Portugal after the arrival of the *corpi santi*, as seen in German-speaking countries, or if they were imported from Italy already mounted as *simulacra*. Both *simulacra* incorporated bones from multiple individuals, a practice documented in the literature, reinforcing the common use of composite skeletons in such assemblages. Martyrdom symbols, such as flower crowns, further differentiate the *simulacra*. St. Primogenita's crown is adorned with fabric petals, while St. Theodore's crown is made of coloured cellulosic materials, reflecting distinct patterns in their material construction.

The fabrics used in the garments, including both coloured fibres and metal threads, exhibit significant degradation, which is evident in colour fading and metal corrosion. SEM–EDS and Py-GC–MS analyses of St. Primogenita's phial of blood revealed what appears to be a creative technique employed to enhance the appearance of the blood within the phial. This addition underscores the phial's symbolic role, emphasising the sanctity and martyrdom of the *simulacrum*.

Simulacra represent a forgotten religious heritage, and the material examination, supported by the historical research in this work, intended to highlight these valuable artefacts. This study uncovered two impressive examples from a set of seven at the Santa Casa de Misericórdia de Almada (Portugal), providing a framework for future investigations into the historical, conservation, and material contexts of *corpi santi*.

Supplementary Information The online version contains supplementary material available at https://doi.org/10.1140/epjp/s13360-025-06356-3.

Acknowledgements The authors extend their heartfelt gratitude to Dr Paula Costa and the Social Bodies of Santa Casa da Misericórdia de Almada for granting access to the *simulacra* during the various in situ campaigns and creating the conditions for their successful execution. We also thank Dr Paula Costa for her invaluable archival research on the placement of the *simulacra* since their arrival at SCMA and for generously sharing this information with us. We also acknowledge Dr Rui Mendes for historical information on the relics. We thank Prof Armando Senra Martins for his valuable help with the Latin language and Marius Araújo for the photographs of St. Primogenita seal. We also acknowledge FCT for funding through the "Holy Bodies" Project (https://doi.org/10.54499/2022.01486.PTDC), J. Palmeirão and M. Nunes research fellowship and studentship, respectively. Ana Manhita and Ana Curto acknowledge FCT for financial support (https://doi.org/10.54499/CEECIND/00791/2017/CP1431/CT0005 and https://doi.org/10.54499/2020.02110.CEECIND/CP1593/CT0005, respectively). Funding was also provided through the strategic projects https://doi.org/10.54499/UIDP/04449/2020, https://doi.org/10.54499/UIDB/04449/2020, and IN2PAST https://doi.org/10.54499/LA/P/0132/2020 (HERCULES Laboratory), UIDB/0622/2020 and UIDP/0622/2020 (CITAR), and UIDB/00057/2020, UIDP/00057/2020 (CIDEHUS).

Author contributions Teresa Ferreira, Joana Palmeirão, Margarida Nunes, and Eduarda Vieira performed conceptualisation; Teresa Ferreira and Margarida Nunes were involved in methodology design and samples preparation; Teresa Ferreira, Margarida Nunes, and Ana Curto participated in investigation; Luís Piorro was responsible for in situ radiographic imaging; Margarida Nunes took part in visualisation, digital microscopy, SEM-EDS, FT-IR analysis, and data curation; Teresa Ferreira and Ana Manhita were involved in HPLC–DAD-MS and Py-GC–MS analysis and data curation; Teresa Ferreira, Margarida

Nunes, Ana Curto, and Fernanda Olival performed writing—original draft preparation. All authors were involved in writing—reviewing. All authors have read and approved the final manuscript.

Funding Open access funding provided by FCT|FCCN (b-on).

Data Availability Statement The authors declare that the data supporting the findings of this study are available within the paper and its supplementary information file. Should any raw data files be needed in another format, they are available from the corresponding author upon request. The manuscript has associated data in a data repository.

Declarations

Conflict of interest The authors have no relevant financial or non-financial interests or competing interests to declare that are relevant to the content of this article.

References

1. University of Notre Dame, Martyrology—the demographics of Christian martyrdom. https://mcgrath.nd.edu/ (2010)
2. F.L. Cross, E.A. Livingstone, *The Oxford Dictionary of the Christian Church*, 3rd edn. (Oxford University Press, New York, 2005)
3. J.B. Rives, *The Obligations of Empire: Decius to the Tetrarchs*, online. (Oxford Academic, New York, 2024)
4. L. Misiarczyk, in *Ser. Byzantina - Stud. Byzantine Post-Byzantine Art*, edited by W. Deluga (Polish Institute of World Art Studies | Cardinal Stefan Wyszyński University, Warsaw, 2016), pp. 13–23
5. J. L. Osborne, JSTOR **53**, 278 (1985). http://www.jstor.org/stable/40310821
6. T. Head, *The Cult of the Saints and Their Relics* (2013), pp. 1–12.
7. M. Ghilardi, in *Cardinal Montelpare—Atti Del Convegno* (Archivio Diocesano San Benedetto del Tronto, Montelparo, 2013), p. 99.
8. S. Baciocchi, C. Duahmelle, *Reliques Romaines* (Publications de L' École Francaise de Rome, 2016). https://doi.org/10.4000/books.efr.40192
9. M. Ghilardi, Arch. Sci. Soc. Relig. 167 (2018). https://doi.org/10.4000/assr.38845
10. G. Reyes, Examinan Relicarios de Ceroplástica de La Catedral Metropolitana y de San Ángel. https://retodiario.com/cultura/2016/07/05/examinan-relicarios-de-ceroplastica-de-la-catedral-metropolitana-y-de-san-angel/; https://www.youtube.com/watch?v=7xGalSGdGFQ (2016)
11. F. Ciappara, Hist. Reflect. **43**, 1 (2017)
12. N. Litaker, Church Hist. **89**, 801 (2020). https://doi.org/10.1017/S0009640721000020
13. J. Palmeirão, E. Vieira, M. Pintado, P. Moreira da Costa, and P. Monteiro, in *Jornadas Investig. Emerg. En Conserv. y Restauración Patrim* (2014), pp. 423–432.
14. L. Biehler-Gomez, D. Porta, M. Mattia, D. De Angelis, P. Poppa, C. Cattaneo, Int. J. Osteoarchaeol. **31**, 506 (2021). https://doi.org/10.1002/oa.2967
15. F. Dedouit, G. Guglielmi, G. Perilli, M. Nasuto, N. Telmon, V. Fineschi, C. Pomara, J. Forensic Radiol. Imaging **2**, 9 (2014). https://doi.org/10.1016/j.jofri.2013.11.006
16. P. Koudounaris, *Heavenly Bodies Cult Treasures and Spectacular Saints from the Catacombs* (Thames & Hudson, New York, 2013)
17. A. Petaros, M. Cavka, A. Skrobonja, in *Bulletin of the International Association for Paleodontology* (2011), pp. 28–35.
18. N. Prader, Reliquiengebeine – Nur Überreste Eines Toten? Dekomposition, Schadensursachen Und Konsolidierung Am Beispiel Des Katakombenheiligen Placide, Scuola universitaria professionale della Svizzera italiana (2012)
19. J. Palmeirão, Simulacra Corporum Sanctorum Martyrum - Estudo de Um Património Em Risco e Estratégias Para a Sua Valorização e Salvaguarda, Universidade Católica do Porto, PhD thesis. http://hdl.handle.net/10400.14/43164 (2023)
20. J. Imagem-Relicário de Santo Aurélio Mártir Pertencente à Sé Catedral Do Porto. Estudo e Conservação Integrada Das Relíquias, Universidade Católica do Porto, Master dissertation. http://hdl.handle.net/10400.14/18900 (2015)
21. L.A. Kristóf, M. Kovács, G. Baksa, Z. Bereczki, F. Szatmári, L. Patonay, G. Pálfi, L. Pohárnok, J. Cult. Herit. **16**, 249 (2015). https://doi.org/10.1016/j.culher.2014.04.001
22. G. Reyes, La Donación de Corpi Santi En México Siglos XVI – XIX, El Colegio de Michoacán, PhD thesis. http://colmich.repositorioinstitucional.mx/jspui/handle/1016/1458 (2021)
23. A.C. Pfeiffer, Auferweckt in Herrlichkeit! Barocke Heilige Leiber in Oberschwaben: Materialien, Fixierungstechniken, Konservatorische Aspekte (2005)
24. A. Alterauge, T. Becker, B. Berndt, C. Jackowski, S. Lösch, Radiographics **36**, 573 (2016). https://doi.org/10.1148/rg.2016150008
25. K.L. Rasmussen, J. van der Plicht, J. La Nasa, E. Ribercini, M.P. Colombini, T. Delbey, L. Skytte, S. Schiavone, U. Kjær, P. Grinder-Hansen, L.R. Lanzillotta, Herit. Sci. **9**, 1 (2021). https://doi.org/10.1186/s40494-021-00481-9
26. Y. Nie, E. Kleine-Benne, O.O. Sonibare, T. Hoffmann, S.F. Foley, Thermochemolysis—a simple and rapid methylation method based on TMAH for Gas Chromatographic analysis of linseed oil and amber, (Pyro core AppNote, Gerstel 1). https://www.gerstel.com/sites/default/files/2024-04/AppNote-165.pdf
27. M.R. Schilling, A. Heginbotham, H. Van Keulen, M. Szelewski, Stud. Conserv. **61**, 3 (2016). https://doi.org/10.1080/00393630.2016.1230978
28. H. van Keulen, M. Schilling, Stud. Conserv. **64**, S74 (2019). https://doi.org/10.1080/00393630.2019.1594580
29. M.R. Schilling, K. Fritza, S. Phillips, in *Criminalist* (Los Angeles, 2020), p. 1.
30. J. Palmeirão, M. Coutinho, E. Vieira, T. Ferreira, in Relíquias Em Projeto (Museu de São Roque, Lisboa, 2022), p. 27.
31. C. dos Arcos, *Caparica Através Dos Séculos* (Gráfica Progressiva, Cacilhas, 1972)
32. Arquivo Histórico da SCMA, Inventário*s*, Pt.7 (1948, 1949)
33. Archives Downside Abbey-St James the Great, 3 (2020). https://www.flickr.com/photos/downsideabbeyarchives/albums/72157652397127011/
34. P.J. Reimer, Quat. Res. **96**, 22 (2020)

35. M. Galli, Christian History Institute - Persecution in the Early Church: A gallery of the persecuting emperors (1990). https://christianhistoryinstitute.org/
36. L. Scheuer, S. Black, *Development of Juvenile Osteology* (Elsevier Academic Press, San Diego, 2000)
37. H.F.V. Cardoso, J. Abrantes, L.T. Humphrey, Int. J. Legal Med. **128**, 809 (2014). https://doi.org/10.1007/s00414-013-0925-5
38. S.J. AlQahtani, M.P. Hector, H.M. Liversidge, Am. J. Phys. Anthropol. **142**, 481 (2010). https://doi.org/10.1002/ajpa.21258
39. M. Boulet-Audet, F. Vollrath, C. Holland, J. Exp. Biol. **218**, 3138 (2015). https://doi.org/10.1242/jeb.128306
40. X.M. Zhang, P. Wyeth, Sci. China Chem. **53**, 626 (2010). https://doi.org/10.1007/s11426-010-0050-y
41. L. Geminiani, F.P. Campione, C. Canevali, C. Corti, B. Giussani, G. Gorla, M. Luraschi, S. Recchia, L. Rampazzi, Materials. **16** (2023). https://doi.org/10.3390/ma16051819
42. A. Barth, Biophys. Mol. Biol. **74**, 141 (2000). https://doi.org/10.1016/S0079-6107(00)00021-3
43. J. Gu, Q. Li, B. Chen, C. Xu, H. Zheng, Y. Zhou, Z. Peng, Z. Hu, B. Wang, Sci. Rep. **9**, 1 (2019)
44. R.F.P. Pereira, M.M. Silva, V. De Zea Bermudez, Macromol. Mater. Eng. **300**, 1171 (2015). https://doi.org/10.1002/mame.201400276
45. L. Andadari, D. Yuniati, B. Supriyanto, Murniati, S. Suharti, A. Widarti, E. Steven, A. Sadapotto, B. Winarno, Minarningsih, R. Agustarini, N. Muin, W. Isnan, Y. Heryati, Y. Adalina, I. Yeny, R. Dewi, A. Nurlia, S.D. Riendriasari, K.E. Maharani, L.M. Nugraha, B.H. Narendra, Insects **13** (2022). https://doi.org/10.3390/insects13100913
46. Y. Liu, A. Wang, J. Freeman, in *40th Lunar an Planet. Sci.* (Washington University, Saint Louis, 2009), pp. 2128–2129
47. S. Gunasekaran, G. Anbalagan, S. Pandi, J. Raman Spectrosc. **37**, 892 (2006). https://doi.org/10.1002/jrs.1518
48. M. Roy, S.K. Meena, T.S. Kusurkar, S.K. Singh, N.K. Sethy, K. Bhargava, S. Sarkar, M. Das, Biointerphases **7**, 1 (2012). https://doi.org/10.1007/s13758-012-0045-7
49. M. Gauza-Włodarczyk, L. Kubisz, D. Włodarczyk, Int. J. Biol. Macromol. **104**, 987 (2017). https://doi.org/10.1016/j.ijbiomac.2017.07.013
50. R.P. Evershed, World Archaeol. **25**, 74 (1993). https://doi.org/10.1080/00438243.1993.9980229
51. J.D. Rodriguez-Blanco, S. Shaw, L.G. Benning, Nanoscale **3**, 265 (2011). https://doi.org/10.1039/c0nr00589d
52. J.N. Nouping Fekoua, P. Venyite, S. Bila, E. Kamseu, G. Bebga, M. Hanuskova, G. D. Poggetto, S. Rossignol, C. Leonelli, Heliyon **9**, e17750 (2023). https://doi.org/10.1016/j.heliyon.2023.e17750
53. A. Manhita, T. Ferreira, A. Candeias, C. B. Dias, Anal. Bio. Chem. **400**, 1501 (2011). https://doi.org/10.1007/s00216-011-4858-x
54. L. Dussubieux, M.W. Ballard, Mater. Res. Soc. Online Proc. Libr. **852**, 124 (2005). https://doi.org/10.1557/PROC-852-OO4.1
55. E.S.B. Ferreira, A.N. Hulme, H. McNab, A. Quye, Chem. Soc. Rev. **33**, 329 (2004). https://doi.org/10.1039/B305697J
56. M.P. Yuldashev, E.K. Batirov, V.M. Malikov, N.P. Yuldasheva, Chem. Nat. Compd. **32**, 923 (1996)
57. D. A. Peggie, J. Kirby, J. Poulin, W. Genuit, J. Romanuka, D.F. Wills, D. Simone, A.N. Hulme, Anal. Methods **1** (2018). https://doi.org/10.1039/C7AY02626A
58. A.M. A.M. Hacke, C. M. Carr, and A. Brown, in *Proc. Met. Nation Museum of Australia*, (National Museum of Australia, Canberra, 2004), pp. 415–426. https://doi.org/10.13140/RG.2.2.32890.08646
59. K. Tronner, A.G. Nord, J. Sjöstedt, H. Hydman, Stud. Conserv. **47**, 109 (2002). https://doi.org/10.1179/sic.2002.47.2.109
60. T. Ferreira, H. Moreiras, A. Manhita, P. Tomaz, J. Mirão, C.B. Dias, A.T. Caldeira, Microsc. Microanal. **21**, 2 (2015). https://doi.org/10.1017/S1431927614013440
61. A. Karatzani, X-Ray Spectrom. **37**, 410 (2008). https://doi.org/10.1002/xrs.1021
62. V. Muros, S.K.T.S. Wärmländer, D.A. Scott, J.M. Theile, J. Am. Inst. Conserv. **46**, 229 (2007). https://doi.org/10.1179/019713607806112305
63. M. Bergstrand, E. Hedhammar, A.G. Nord, K. Tronner, in *12th Trienn. Meet. ICOM Comm. Conserv*. (1999), pp. 621–624.
64. M. Hacke, Investigation into the Nature and Ageing of Tapestry Materials, PhD Thesis, (2006). https://doi.org/10.13140/RG.2.2.32890.08646
65. N.A.R. van Giffen, S.P. Koob, Encycl. Archaeol. Sci. **1** (2018). https://doi.org/10.1002/9781119188230.saseas0179
66. R. Zanini, G. Franceschin, E. Cattaruzza, A. Traviglia, Mater. Degrad. **7**, 1 (2023). https://doi.org/10.1038/s41529-023-00355-4
67. W.W. Meyer, J. Ecclesiast. Hist. **46**, 75 (1995). https://doi.org/10.1017/S0022046900012550
68. A. Barth, Biochim. Biophys. Acta Bioenerg. **1767**, 1073 (2007). https://doi.org/10.1016/j.bbabio.2007.06.004
69. M. Regert, S. Colinart, L. Degrand, O. Decavallas, Archaeometry **43**, 549 (2001). https://doi.org/10.1111/1475-4754.00036
70. M. Vandenbeusch, R. Stacey, D. Antoine, J. Archaeol. Sci. Rep. **40**, 103186 (2021)
71. M. Regert, J. Langlois, E. Laval, A.S. Le Hô, S. Pagès-Camagna, Anal. Chim. Acta **577**, 140 (2006). https://doi.org/10.1016/j.aca.2006.06.038
72. A. Lattuati-Derieux, S. Thao, J. Langlois, M. Regert, J. Chromatogr. A **1187**, 239 (2008). https://doi.org/10.1016/j.chroma.2008.02.015
73. A.M. Cardoso, I. Crina, A. Sandu, E. Sandbakken, A. Manhita, S. Valadas, C. Dias, A. Candeias, Int. J. Conserv. Sci. **13**, 1665 (2022)
74. Y. Le Conte and M. Navajas, Reveu Sci. Tech. **27**, 485 (2008). https://doi.org/10.20506/rst.27.2.1819